Front. Mater. Sci. 2022, 16(1): 220586
https://doi.org/10.1007/s11706-022-0586-8

RESEARCH ARTICLE

High-performance fiber strain sensor of carbon nanotube/thermoplastic polyurethane@styrene butadiene styrene with a double percolated structure

Dong XIANG (✉)[1,2*], Libing LIU[1*], Xiaoyu CHEN[1], Yuanpeng WU[1,5], Menghan WANG[3], Jie ZHANG[4], Chunxia ZHAO[1], Hui LI[1], Zhenyu LI[1], Ping WANG[1], and Yuntao LI (✉)[1,2]

1 School of New Energy and Materials, Southwest Petroleum University, Chengdu 610500, China
2 State Key Laboratory of Oil and Gas Reservoir Geology and Exploitation, Southwest Petroleum University, Chengdu 610500, China
3 College of Materials Science and Engineering, Chongqing University, Chongqing 400030, China
4 School of Mechatronic Engineering, Southwest Petroleum University, Chengdu 610500, China
5 The Center of Functional Materials for Working Fluids of Oil and Gas Field, Southwest Petroleum University, Chengdu 610500, China

ABSTRACT: In this work, a high-performance fiber strain sensor is fabricated by constructing a double percolated structure, consisting of carbon nanotube (CNT)/thermoplastic polyurethane (TPU) continuous phase and styrene butadiene styrene (SBS) phase, incompatible with TPU (CNT/TPU@SBS). Compared with other similar fiber strain sensor systems without double percolated structure, the CNT/TPU@SBS sensor achieves a lower percolation threshold (0.38 wt.%) and higher electrical conductivity. The conductivity of 1%-CNT/TPU@SBS (4.12×10^{-3} S·m^{-1}) is two orders of magnitude higher than that of 1%-CNT/TPU (3.17×10^{-5} S·m^{-1}) at the same CNT loading of 1 wt.%. Due to double percolated structure, the 1%-CNT/TPU@SBS sensor exhibits a wide strain detection range (0.2%−100%) and an ultra-high sensitivity (maximum gauge factor (GF) is 32411 at 100% strain). Besides, the 1%-CNT/TPU@SBS sensor shows a high linearity (R^2 = 0.97) at 0%−20% strain, relatively fast response time (214 ms), and stability (500 loading/unloading cycles). The designed sensor can efficiently monitor physiological signals and movements and identify load distribution after being woven into a sensor array, showing broad application prospects in wearable electronics.

KEYWORDS: double percolated structure; strain sensor; fiber; carbon nanotube; nanocomposite

Contents

Received October 7, 2021; accepted December 20, 2021

E-mails: dxiang01@hotmail.com (D.X.), yuntaoli@swpu.edu.cn (Y.L.)

* D.X. and L.L. contributed equally to this work.

1 Introduction

As indispensable wearable electronic devices, flexible strain sensors have attracted extensive interest in the fields of human motion detection, medical health monitoring systems, intelligent robotics, and human-machine interactions [1–4]. Recently, much research has been done to improve the performance of strain sensors, including mechanical, electrical and sensing properties, by integrating conductive nanofillers (carbon black (CB) [5], carbon nanotubes (CNTs) [6–7], graphene and its derivatives [8–9], MXene [10], metallic nanowires/nanoparticles [11–12] and their hybrids) and elastic matrix materials (polydimethylsiloxane (PDMS) [13–14], polyurethane (PU)/thermoplastic polyurethane (TPU) [15–17], and styrene butadiene styrene (SBS) [18–19]). Light, highly stretchable, and flexible strain sensors [20–21], based on conductive polymer composites (CPCs), are suitable for the development of wearable electronics. In addition, fiber strain sensors are embedded in textile or clothing through knitting technology [22–23] to monitor human movement and health, and to better meet various environmental applications. Therefore, fiber strain sensors are popular among researchers [11,24–26].

High-performance strain sensors usually require a wide strain detection range and high sensitivity as their key performance parameters [6,27]. Wang et al. [28] prepared PDMS/CNT decorated wearable fiber strain sensor and achieved a 100% strain detection limit, while its maximum gauge factor (GF) was just 0.339. Yang et al. [29] fabricated a 3D helical copper/PU/cyanoacrylate fiber that exhibited a large strain detection limit (200%) but low sensitivity (maximum GF of about 0.0005). Although most of these fiber strain sensors exhibit a large strain detection limit, their sensitivity is low, with GFs usually less than 50 [17,25–26,28]. Low sensitivity limits their application in health monitoring systems and intelligent robotics, which need accurate and sensitive signal capture. To solve this problem, Hu et al. [30] developed a highly sensitive (maximum GF of 1127) graphene/CNT/PDMS fiber strain sensor, but its strain detection range was low (3.1%). Effectively integrating a wide strain detection range and high sensitivity is still a challenge for development of high-performance fiber strain sensors.

Many researchers have made efforts to improve the strain detection range and sensitivity. Yu et al. [18] prepared a CNT/SBS fiber strain sensor, using π–π interaction between CNTs and SBS to achieve a wide strain detection range (5%–267%) and high sensitivity (maximum GF of 2889). However, the minimum detectable strain of the sensor was not low enough to accurately and sensitively detect the signals of subtle strain. Yue et al. [31] improved the sensitivity (maximum GF of 28084) of the CB/TPU fiber strain sensors with a 10%–200% strain detection range by using a porous core−sheath structure. Nevertheless, it exhibited low sensitivity (about 0.07) at 10% strain and could not detect lower strain limits. Chen et al. [32] fabricated CNT/TPU composites by non-covalent modification of CNTs coated on commercial spandex fiber. The resulting fiber strain sensor showed a wide strain detection range (1%–200%) and high sensitivity (maximum GF of 14191.5). Several fiber strain sensors with a wide strain detection range and high sensitivity have been developed by interfacial interactions [18–19,32] and core−sheath structures [31]. However, the low strain detection limit rarely breaks below 1%, limiting the application of fiber strain sensors in subtle strain detection [33–34]. In addition, organic solvents used in fiber preparation are toxic or carcinogenic, and can damage the human body and the environment. Moreover, the high costs and complexity of preparing fiber stock solutions have received little research attention.

Many studies introduced double percolated structures into CPCs to reduce the percolation threshold. Liu et al. [35] reported a two-step "*in situ* microfibrillation" and "microfiber coalescence" strategy to achieve a double percolated network of a polybutene-1/polystyrene/CNTs ternary system and achieved a percolation threshold of 0.5 wt.%. Bizhani et al. [36] reported a polycarbonate/polystyrene-co-acrylonitrile/CNTs with a percolation threshold of 0.4 wt.%. Mao et al. [37] prepared CPCs with the same low percolation threshold of 0.5 wt.% using blends filled with polystyrene, poly(methyl methacrylate), and octadecylamine-functionalized graphene. To the best of the authors' knowledge, very few studies have reported on the effect of double percolated structure on the sensing performance of fiber strain sensors.

Herein, we report a low-cost and simple strategy to fabricate high-performance fiber strain sensors by constructing a double percolated structure consisting of CNT/TPU continuous phase and SBS phase incompatible with

TPU. The CNT/TPU@SBS fiber strain sensor achieves a wide strain detection range, an ultra-high sensitivity, and a low percolation threshold. In addition, the sensor shows high linearity (for 0%–20% strain), relatively fast response time, excellent stability, and monitors different strains/frequencies. CNT/TPU@SBS is assembled to monitor human movement and identify the load distribution, demonstrating its potential in wearable electronics and intelligent systems.

2 Experimental

2.1 Materials

CNTs (NC7000, 90%) with a density of 1.85 $g \cdot cm^{-3}$ were purchased from Nanocyl SA (Belgium). The average diameter and length of CNTs were 9.5 nm and 1.5 μm, respectively. TPU particles (Bayer 2195) were obtained from Bayer Co. Ltd. (Germany) with a melt flow index of 12.1 g/10 min (at 205 °C under a 5 kg load) and a density of 1.19 $g \cdot cm^{-3}$. SBS particles (YH-792) with a melt flow index of 1.5 g/10 min (at 200 °C under a 5 kg load) and a density of 0.92 $g \cdot cm^{-3}$ were supplied by Baling Petrochemical Corporation, SINOPEC (China). Dichloromethane (DCM) was obtained from Chengdu Cologne Chemical Reagent Company (China).

2.2 Preparation of fiber strain sensors

The preparation scheme for CNT/TPU@SBS fibers with the double percolated structure is shown in Figs. 1(a) and 1(b). TPU was added to a computer-controlled torque rheometer (ZJL-200), heated, and mixed for 5 min at 160 °C and 60 $r \cdot min^{-1}$. CNTs were added to the torque rheometer and mixed for another 5 min. Then SBS (mass ratio of *m*(SBS):*m*(TPU) = 1:1) was added to mix for 3 min to obtain CNT/TPU@SBS composite. Shorter SBS mixing time avoids the transfer of CNTs from TPU to SBS. Subsequently, CNT/TPU@SBS sheet was obtained by hot pressing at 180 °C and 10 MPa. After granulation, the particles were extruded into filaments with a diameter of 1.75 mm by a benchtop single screw extruder (Wellzoom Type C) at an operating temperature of 190 °C and a screw speed of 60 $r \cdot min^{-1}$ (Fig. 1(a)). The filaments were fed into an ET-K1 (ET Co. Ltd., China) desktop fused filament fabrication (FFF) 3D printer to fabricate the CNT/TPU@SBS fibers with a double percolated structure at 200 °C. The internal conductive network structure of CNT/TPU@SBS fibers is illustrated in Fig. 1(b). Figure 1(c) shows the photographs of CNT/TPU@SBS fibers.

For CNT/TPU fibers, the same preparation method was used. Specifically, TPU was added to the torque rheometer, heated, and mixed for 5 min at 160 °C and 60 $r \cdot min^{-1}$. CNTs were added and mixed for 8 min to obtain CNT/TPU

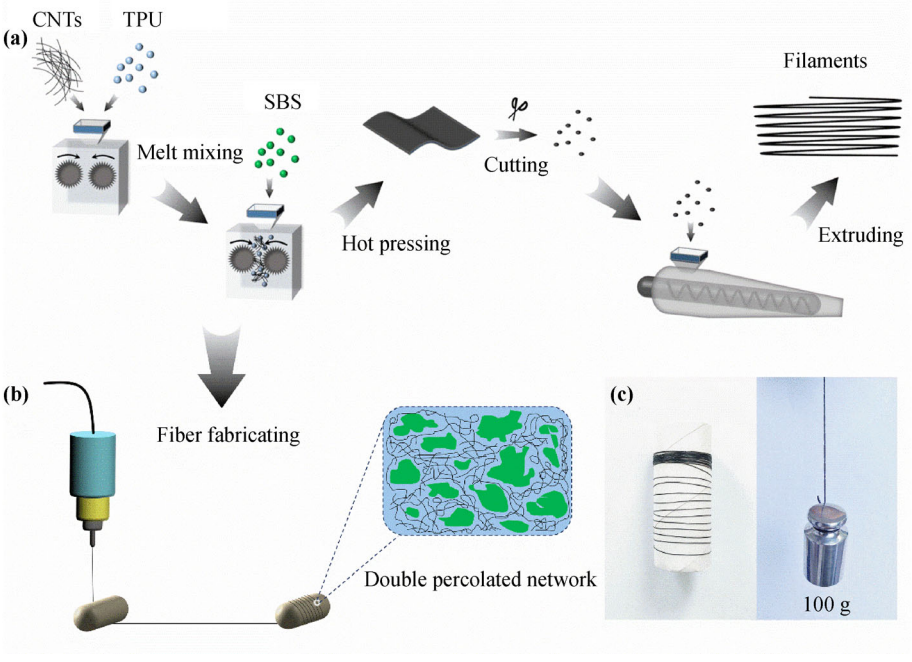

Fig. 1 **(a)(b)** Schematic diagram for the preparation process and double percolated network of CNT/TPU@SBS. **(c)** Photographs of CNT/TPU@SBS.

composite.

The fibers were connected to two silver wire electrodes with a distance of 30 mm, and conductive silver paste was coated on the electrodes to eliminate contact resistance, so as to obtain fiber strain sensors. Fibers with a double percolated structure are denoted as *x*-CNT/TPU@SBS, where *x* represents the weight percentage of CNTs in the system. For example, 1%-CNT/TPU@SBS indicates that the system contains 1 wt.% CNTs.

2.3 Characterization

The microscopic morphology was studied by scanning electron microscopy (SEM; ZEISS EV0 MA15) at an accelerating voltage of 20 kV. Before the SEM analysis, the fibers were etched with DCM solution to eliminate the SBS phase. The cross-section of the fractured fibers, without platinum sputtering, was used to observe the CNTs dispersion within the composite. The conductive network, based on rich secondary electrons emitted from the conductive CNTs, was observed.

The electrical conductivity (σ) of fiber strain sensors was measured using a two-point method [38], combined with a direct current (DC) digital source meter (Tektronix PWS4323) and picoamp-meter (Keithley 6485) at 3 V. The conductivity of fiber strain sensors was calculated using following Eq. (1):

$$\sigma = \frac{L}{RS} \tag{1}$$

where R is the resistance; and L and S are the electrode distance and the cross-sectional area of the fiber strain sensor, respectively.

The sensing performance was tested by combining a universal tester (MTS CMT4104) with the above mentioned digital source meter and picoamp-meter at 3 V. The distance between the electrodes was adjusted to 30 mm. The fibers were clamped on the universal tester and connected to the data recording system to study the relationship between strain and relative resistance change ($\Delta R/R_0$). The sensitivity (known as GF) of fiber strain sensors was calculated using Eq. (2):

$$\mathrm{GF} = \frac{\Delta R}{R_0} \times \frac{1}{\varepsilon} \tag{2}$$

where ε, ΔR, and R_0 represent the applied strain, the resistance change under strain, and the initial resistance, respectively.

3 Results and discussion

3.1 Morphology

The morphologies of the fiber strain sensors are shown in Fig. 2. Figures 2(a) (2(a′))–2(f) (2(f′)) represent 1 wt.% CNT/TPU, 2 wt.% CNT/TPU, 3 wt.% CNT/TPU, 1 wt.% CNT/TPU@SBS, 2 wt.% CNT/TPU@SBS, and 3 wt.% CNT/TPU@SBS, respectively. Bright CNTs on the fracture surface can be observed and with the increase of CNTs wt.%, the conductive network structure becomes more complete. Compared to CNT/TPU system (Figs. 2(a)–2(c)), CNT/TPU@SBS has many holes, indicating SBS was etched by DCM (Figs. 2(d)–2(f)). Dispersion of CNTs is relatively uniform within CNT/TPU composites (Figs. 2(a′)–2(c′)). However, it can be observed that the dispersion of CNTs within the TPU phase is enhanced, and the conductive network is denser at the same CNTs wt.% in the remained CNT/TPU skeletons under a higher magnification (Figs. 2(d′)–2(f′)). The reason for the enhanced dispersion of CNTs could be attributed to the introduction of SBS, which increases the local concentration of CNTs in the more confined region of the TPU phase, resulting in the increased viscosity of TPU melt [39]. Therefore, the shear force increases in the mixing process, facilitating the dispersion of CNTs in the TPU phase [40]. CNTs could be distributed in the TPU phase instead of SBS phase, which can be attributed to the mixing order of the blends [41]. The etched SBS and CNTs distributed within TPU continuous phase indicate the construction of a double percolated structure within CNT/TPU@SBS. Furthermore, the double percolated structure results in a more complete conductive network, which can be also confirmed from the following electrical property testing.

3.2 Electrical properties

The double percolated structure and CNT wt.% significantly affect the electrical conductivity of fiber strain sensors. As shown in Fig. 3(a), 4.12×10^{-3}, 5.89×10^{-2}, 2.36×10^{-1}, 3.17×10^{-5}, 1.65×10^{-2}, and 8.55×10^{-2} $\mathrm{S\cdot m^{-1}}$ are the electrical conductivities of 1%-CNT/TPU@SBS, 2%-CNT/TPU@SBS, 3%-CNT/TPU@SBS, 1%-CNT/TPU, 2%-CNT/TPU, and 3%-CNT/TPU, respectively. Compared with CNT/TPU, the conductivity of CNT/TPU@SBS is higher for a given CNTs wt.%, due to the formation of the double percolated structure. The volume excluded effect of SBS phase increases the density of the

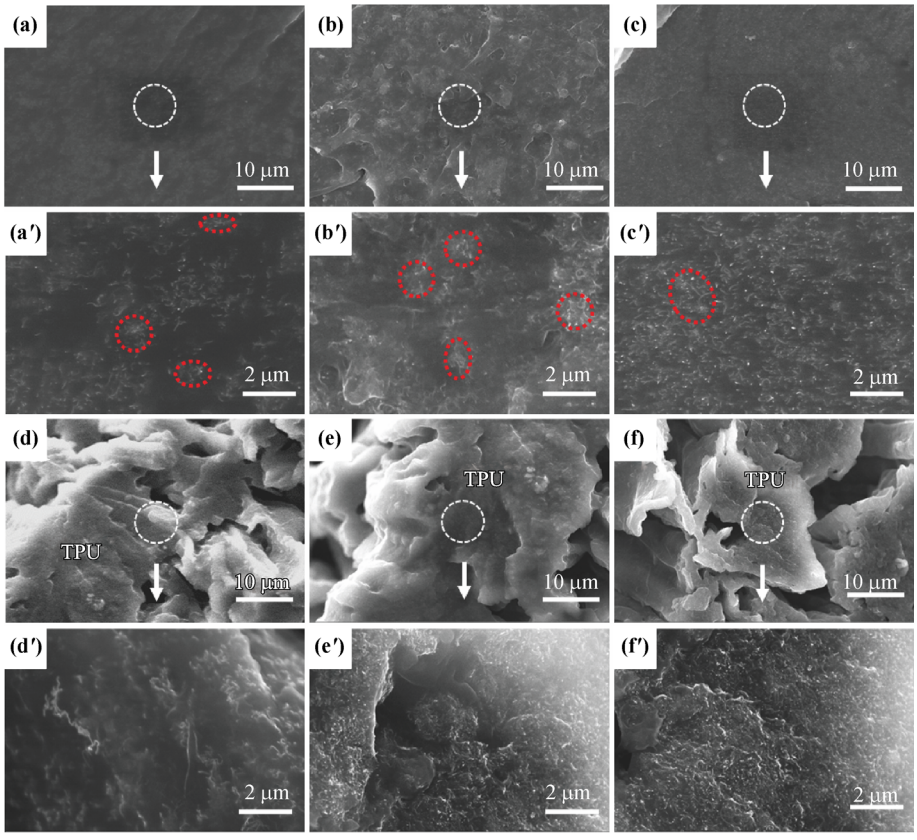

Fig. 2 SEM images of CNT/TPU and CNT/TPU@SBS: **(a)** 1%-CNT/TPU, **(b)** 2%-CNT/TPU, **(c)** 3%-CNT/TPU, **(d)** 1%-CNT/TPU@SBS, **(e)** 2%-CNT/TPU@SBS, and **(f)** 3%-CNT/TPU@SBS. **(a′)(b′)(c′)(d′)(e′)(f′)** Further enlargement of panels (a)–(f), respectively. The CNT agglomerates are circled by red dotted lines.

conductive network of CNTs compared to CNTs directly dispersed within CNT/TPU composite. Particularly, the conductivity of 1%-CNT/TPU@SBS (4.12×10^{-3} S·m^{-1}) is two orders of magnitude higher than that of 1%-CNT/TPU (3.17×10^{-5} S·m^{-1}). In addition, the conductivity of fiber strain sensors increases with the increase in CNTs wt.% and shows a classic percolation behavior. The inset in Fig. 3(a) shows the relationship between the percolation threshold and conductivity according to classical percolation theory, as given in Eq. (3) [42]:

$$\sigma_{\mathrm{p}} = \sigma_0 (p - p_{\mathrm{c}})^t \tag{3}$$

where σ_{p} is the conductivity of CPCs, σ_0 is a scale factor, p is the weight fraction of CNTs, p_{c} is the percolation threshold of CPCs, and t is the critical exponent that depends on the dimension of the conductive network and the materials. The t values range between 1 and 1.3 for two-dimensional (2D) conductive networks and between 1.6 and 2 for three-dimensional (3D) conductive networks [42]. Although some previously reported experimental studies are in good agreement with the theoretical results, t also changes in many practical systems and higher t values indicate the construction of more effective 3D conductive networks [13,43].

According to the experimental data shown in Fig. 3(a), the t values are 5.97 and 5.19 for CNT/TPU@SBS and CNT/TPU (the inset in Fig. 3(a)), respectively, indicating that the CNT/TPU@SBS system probably constructed a more effective 3D conductive networks than the CNT/TPU system [43–44]. It could be attributed to the formation of double percolated structure; that is, the introduction of SBS insulating phase makes the CNT/TPU conductive phase more compact, and the conductive networks constructed by CNTs dispersed in TPU phase are denser. Furthermore, the percolation thresholds of CNT/TPU@SBS and CNT/TPU are 0.38 and 0.50 wt.%, respectively. As expected, the double percolated structure effectively reduces the percolation threshold of CNT/TPU@SBS, which is 24% lower than that of CNT/TPU. This phenomenon is attributed to the fact that CNTs only form a percolation network within TPU continuous phase, rather than the whole composite. Compared with other double percolated systems [45–46],

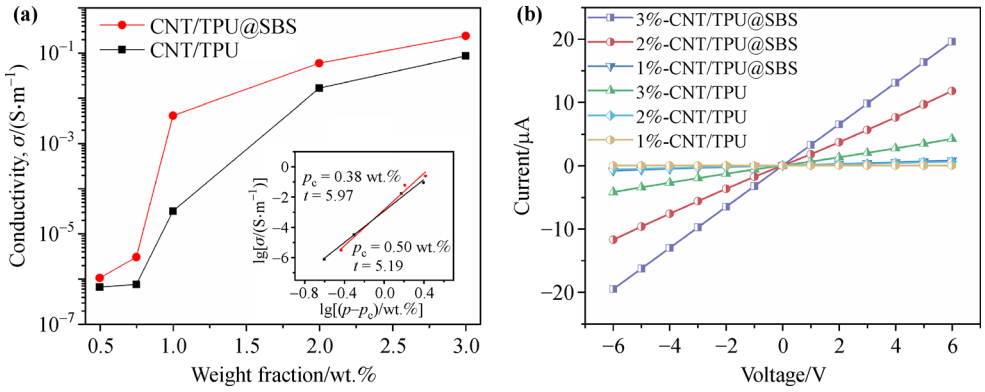

Fig. 3 **(a)** Volume conductivity of CNT/TPU@SBS and CNT/TPU with different CNTs wt.%. **(b)** *U–I* curves for CNT/TPU@SBS and CNT/TPU.

the percolation threshold observed in this work is at a low level.

The *U–I* characteristic relationship of fiber strain sensors is shown in Fig. 3(b). The current linearly increases with the voltage from −6 to 6 V. As shown in Fig. 3(b), the resistance of CNT/TPU@SBS is generally lower than that of CNT/TPU. Specifically, the resistance of fiber strain sensors is in order of 3%-CNT/TPU@SBS < 2%-CNT/TPU@SBS < 3%-CNT/TPU < 1%-CNT/TPU@SBS < 2%-CNT/TPU < 1%-CNT/TPU. This result directly reflects the denser conductive network constructed by CNTs within the TPU continuous phase in the CNT/TPU@SBS system. The SBS phase squeezes the TPU continuous phase, which makes CNTs conductive networks within TPU phase more concentrated (Figs. 2(d′)–2(f′)) and transfers electrons more effectively.

3.3 Sensing performance

Figure 4(a) shows the relationship between the applied strain and $\Delta R/R_0$. The maximum strain detection limits for the CNT/TPU system are less than 100%, precisely 82%, 53%, and 35% for 1%-CNT/TPU, 2%-CNT/TPU, and 3%-CNT/TPU, respectively. This result can be attributed to the increased CNTs agglomeration in a single CNT/TPU phase (Figs. 2(a′)–2(c′)), leading to more stress concentration sites and fiber fracture under strain. However, the maximum strain detection limit of all the CNT/TPU@SBS systems can achieve is 100%. The introduction of the SBS phase improves the stretchability of composites due to the enhancement of CNTs' dispersion (Figs. 2(d′)–2(f′)), increasing the maximum strain detection limit. Moreover, the CNT/TPU@SBS system achieves a higher GF. For example, maximum GF values for 1%-CNT/TPU@SBS, 2%-CNT/TPU@SBS, and 3%-CNT/TPU@SBS are 32411, 16182, and 7767, respectively. These values are much higher than GFs of the CNT/TPU system (45.92, 9.71, and 6.85 for 1%-CNT/TPU, 2%-CNT/TPU, and 3%-CNT/TPU, respectively).

For small strain (0%–20%), GF values of 6.53, 5.02, and 1.57 are obtained, corresponding to 1%-CNT/TPU, 2%-CNT/TPU, and 3%-CNT/TPU, respectively. In comparison, 1%-CNT/TPU@SBS, 2%-CNT/TPU@SBS, and 3%-CNT/TPU@SBS achieve higher GF values of 125, 60.22, and 24.1, respectively (Fig. 4(b)). The higher sensitivity of CNT/TPU@SBS is attributed to the construction of the double percolated structure. Figure 4(c) explains the effect of double percolated structure on the high sensitivity of the sensors under strain. When CNT/TPU@SBS is not stretched, the internal conductive network structure remains intact. When CNT/TPU@SBS is stretched, the SBS phase moves and is oriented along the stretching direction, squeezing and deforming the TPU phase, and destroying the conductive network formed within the TPU phase. The higher sensitivity of CNT/TPU@SBS with lower CNTs wt.% can be attributed to the conductive networks constructed within its TPU continuous phase being more fragile and tending to be deformed.

Due to the introduction of the SBS phase, the double percolated structure is constructed with CNT/TPU phase, resulting in a large maximum strain detection limit and high sensitivity. As shown in Fig. 4(d), the maximum strain detection limit and a maximum sensitivity of the CNT/TPU@SBS are high, compared with a series of fiber strain sensors reported in recent literature [8,15,18–19,24,27–30,32].

As shown in Fig. 4(e), compared with CNT/TPU, the fiber sensors in CNT/TPU@SBS system all exhibit high

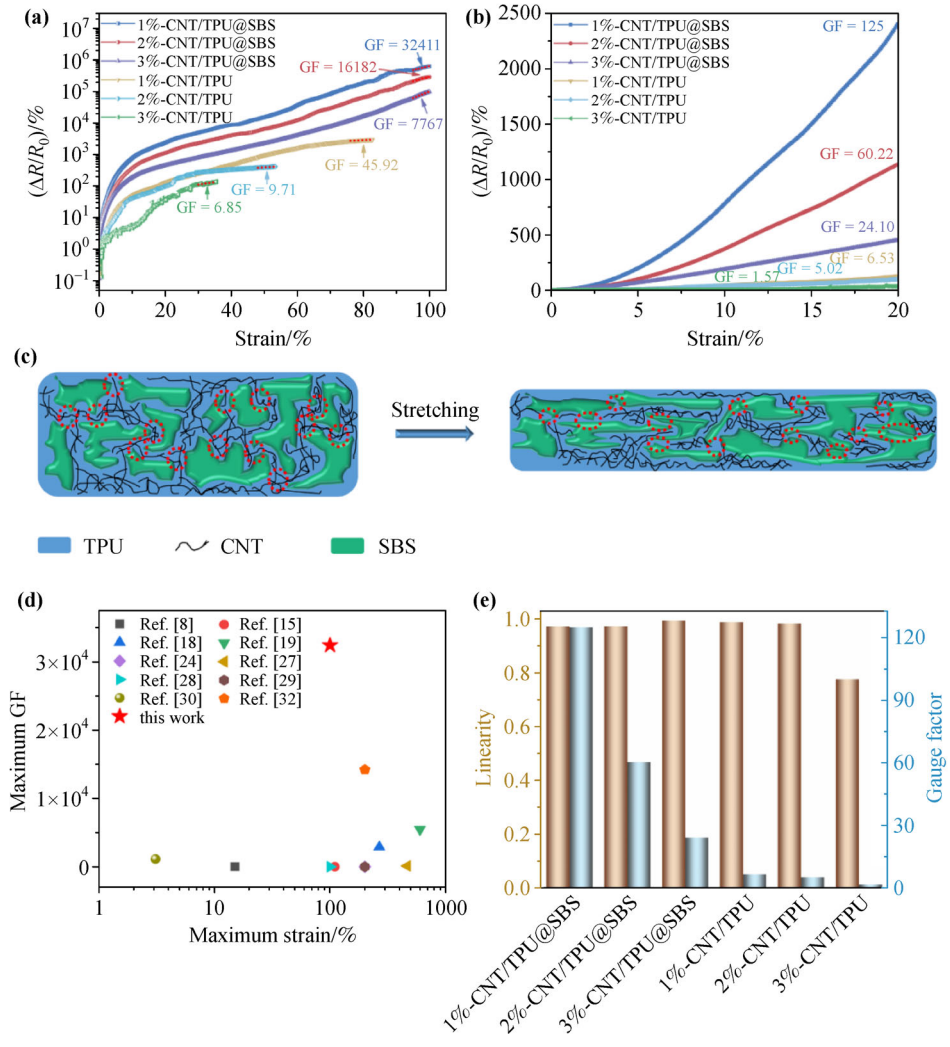

Fig. 4 **(a)(b)** Relationship between $\Delta R/R_0$ and the applied strain. **(c)** Schematic of the conductive network of CNT/TPU@SBS under stretching. **(d)** Comparison of the maximum strain detection limit and the maximum GF of 1%-CNT/TPU@SBS with some reports. **(e)** Linearity and GF comparison between CNT/TPU@SBS and CNT/TPU.

linearity ($R^2 > 0.95$) under applied strain (0%–20%). The linearity ($R^2 = 0.99$) of 3%-CNT/TPU@SBS is higher than that of 2%-CNT/TPU@SBS ($R^2 = 0.97$) and 1%-CNT/TPU@SBS ($R^2 = 0.97$). However, the sensitivity (GF = 125) of 1%-CNT/TPU@SBS is higher than those of 2%-CNT/TPU@SBS (GF = 60.22) and 3%-CNT/TPU@SBS (GF = 24.1) at 20% strain.

The authors further characterize the response time of CNT/TPU@SBS and their electrical signal response under different strains and frequencies. As shown in Fig. 5(a), 1%-CNT/TPU@SBS shows a faster response time (τ_1 = 214 ms) compared to 2%-CNT/TPU@SBS (τ_2 = 257 ms) and 3%-CNT/TPU@SBS (τ_3 = 293 ms) at 10% strain. In Fig. 5(b), the electrical signal response at f = 0.5, 0.2, 0.1, and 0.05 Hz at 10% strain, and the ability to detect electrical signals at different frequencies is demonstrated. The value of $\Delta R/R_0$ increases with the increase in frequency, indicating the frequency dependence of CNT/TPU@SBS. A decrease in molecular mobility at high frequency leads to mechanical response stiffness, which could be the main reason for frequency dependence [47]. In addition, CNT/TPU@SBS is used to identify different tensile strains, demonstrating good repeatability during the cyclic loading (from 1% to 30%), as shown in Fig. 5(c). The value of $\Delta R/R_0$ of CNT/TPU@SBS increases with the increase in loading strain. Due to higher sensitivity of 1%-CNT/TPU@SBS than those of 2%-CNT/TPU@SBS and 3%-CNT/TPU@SBS, $\Delta R/R_0$ of 1%-CNT/TPU@SBS is also high at the same strain.

Furthermore, a stable electrical signal output is obtained

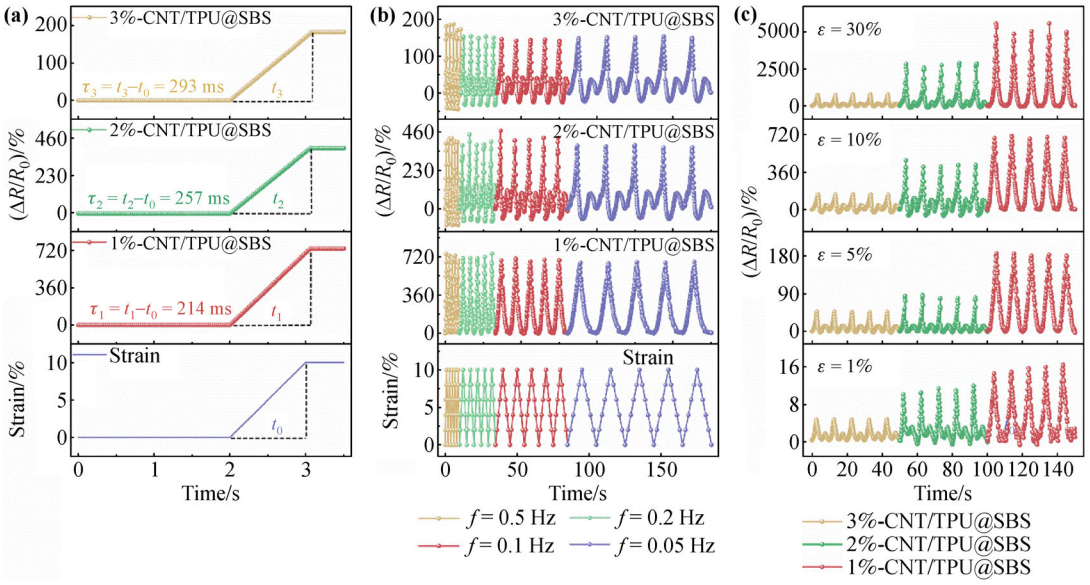

Fig. 5 Sensing performances of CNT/TPU@SBS: **(a)** the response time under uniaxial loading processes; **(b)** variation in $\Delta R/R_0$ during cyclic loading at 10% strain and at frequencies of 0.05, 0.1, 0.2, and 0.5 Hz; **(c)** $\Delta R/R_0$ under loading/unloading cycles under different strains (1%, 5%, 10%, and 30%) at 0.1 Hz.

even under subtle strain of less than 1%, as shown in Fig. 6. With the increasing strain, the value of $\Delta R/R_0$ of CNT/TPU@SBS increases, showing a good resistance response. Some shoulder peaks appear during the cyclic loading and become more obvious with the increase in loading strain. The emergence of shoulder peaks is due to the competitive behavior between the destruction and reconstruction of the conductive network during loading/unloading [6]. The enhanced shoulder peaks are assigned to mechanical hysteresis. After deformation, the retraction of the macromolecular chain leads to the reconstruction of conduction pathways. However, the unloaded macromolecular chain cannot completely return to its original position. This hysteresis leads to the destruction of the conductive network, leading to the emergence of more obvious shoulder peaks [48]. Figure 6 shows that the minimum strain detection limit of 0.2% strain obtained by 1%-CNT/TPU@SBS is lower than that of 2%-CNT/TPU@SBS (0.6%) and 3%-CNT/TPU@SBS (0.8%). This result indicates that 1%-CNT/TPU@SBS has higher sensitivity than 2%-CNT/TPU@SBS and 3%-CNT/TPU@SBS.

To analyze the stability and repeatability of CNT/TPU@SBS, 500 cyclic loading/unloading tests are carried out at a strain of 10% and a frequency of 0.2 Hz. As shown in Fig. 7, 1%-CNT/TPU@SBS, 2%-CNT/TPU@SBS, and 3%-CNT/TPU@SBS have a stable $\Delta R/R_0$ response throughout the test, demonstrating their excellent stability and repeatability.

3.4 Application

1 wt.%-CNT/TPU@SBS may be attached to the human body for monitoring a wide range of movements. Figure 8 (a) shows the real-time resistance response of the sensor

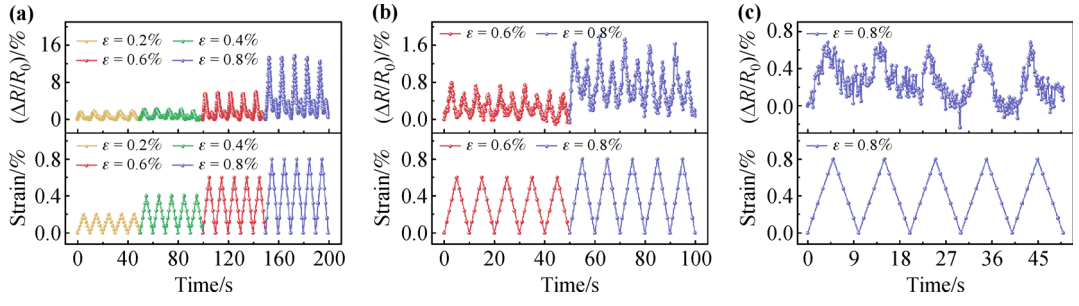

Fig. 6 $\Delta R/R_0$ under loading/unloading cycles with the subtle strain at 0.1 Hz: **(a)** 1%-CNT/TPU@SBS, **(b)** 2%-CNT/TPU@SBS, and **(c)** 3%-CNT/TPU@SBS.

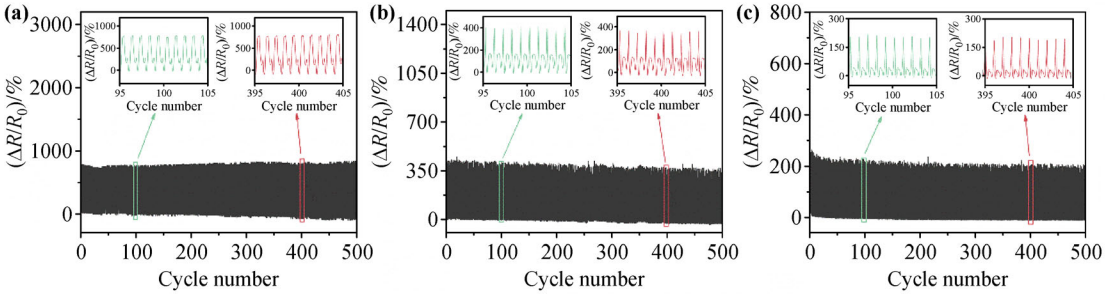

Fig. 7 The stability of **(a)** 1%-CNT/TPU@SBS, **(b)** 2%-CNT/TPU@SBS, and **(c)** 3%-CNT/TPU@SBS during 500 cycles at 10% strain under 0.2 Hz.

monitoring the pulse vibration. The sensor is used to monitor the head deflection, demonstrating its potential application in cervical spondylosis (Fig. 8(b)). The value $\Delta R/R_0$ of the sensor has the potential to reflect how much food is chewed in the mouth (Fig. 8(c)). Furthermore, the $\Delta R/R_0$ response for the finger with different bending degrees is shown in Fig. 8(d). The output electrical signals increase with the increase in bending degree. In addition, the sensor also accurately monitors gestures (Fig. 8(e)). All

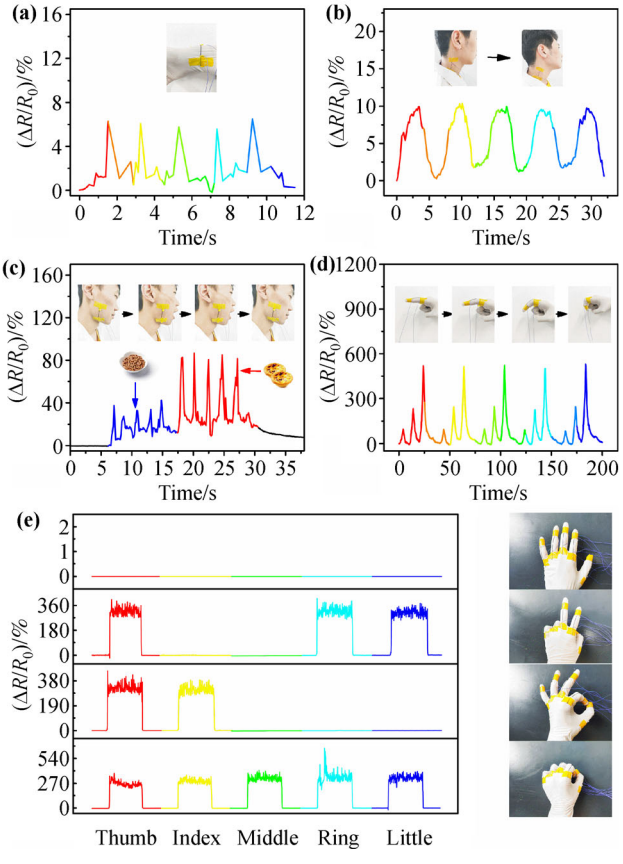

Fig. 8 $\Delta R/R_0$ of 1%-CNT/TPU@SBS in different monitoring applications: **(a)** pulse, **(b)** head deflection, **(c)** chewing, **(d)** finger bending, and **(e)** gesture.

these results demonstrate that 1%-CNT/TPU@SBS has a good application prospect in wearable electronics for monitoring human movements and intelligent robotics.

Moreover, a 5×5 fiber sensor matrix is woven using 1%-CNT/TPU@SBS to explore its application in tactile sensing devices (Fig. 9(a)). Figure 9(d) shows that no physical object is placed on the sensor array, and there is no change in the electrical signal. When the tweezer is placed in the center of the sensor array (Fig. 9(b)), the pressure received at the center is the highest and the electrical signal response is the largest. In addition, the electrical signals decrease with the distance from the center of the sensor array (Fig. 9(e)). When a balance weight is placed in the upper left corner of the sensor array (Fig. 9(c)), the electrical signal response gradually weakens from the upper left corner to the lower right corner of the sensor array (Fig. 9(f)). These results reveal that 1%-CNT/TPU@SBS has enormous potential in tactile sensing.

4 Conclusions

In this study, a high-performance fiber strain sensor is fabricated by introducing the SBS phase, incompatible with the TPU phase, to form a double percolated structure with enhanced electrical and sensing properties. Compared with CNT/TPU without a double percolated structure, CNT/TPU@SBS shows a lower percolation threshold and higher conductivity. 1%-CNT/TPU@SBS exhibits a wide strain detection range (0.2%–100%), an ultrahigh sensitivity (GF = 32411 at a strain of 100%), and high linearity close to 1 (at 0%–20% strain). The sensor shows a relatively fast response time (214 ms), and monitors different strains (1%–30%) and different frequencies (0.05–0.5 Hz). Furthermore, this sensor demonstrates excellent stability throughout 500 cycles. Finally, the fiber strain sensor is used to monitor various human

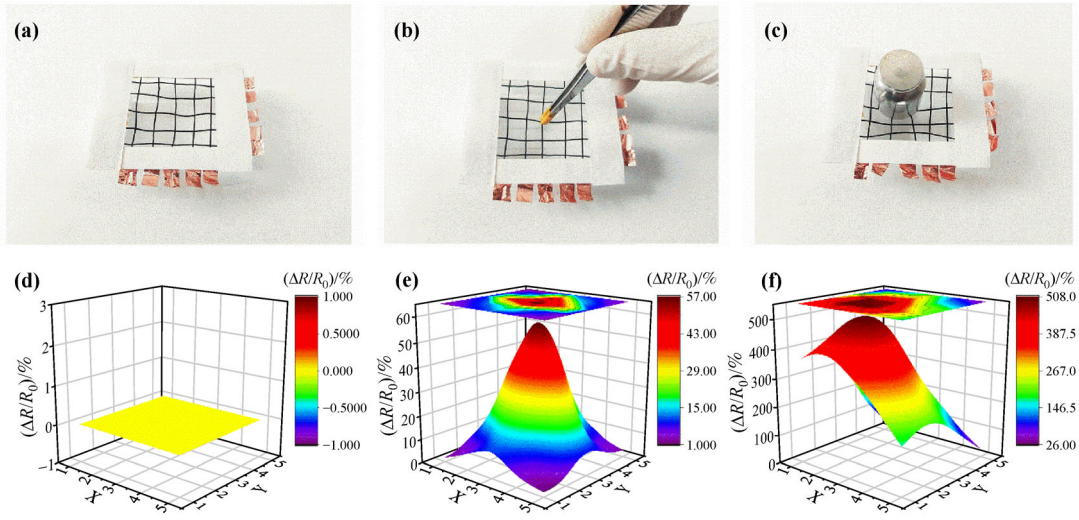

Fig. 9 Photos of **(a)** the sensor array, **(b)** tweezer pressed down on the sensor array, and **(c)** 100 g balance weight placed on the sensor array. $\Delta R/R_0$ of the sensor array in tactile sensing: **(d)** no physical object; **(e)** tweezer; **(f)** balance weight.

movements and identify the load distribution, indicating its promising potential in wearable electronics. The fiber strain sensor with a double percolated structure provides a reference for the development of the next-generation high-performance fiber strain sensors.

Acknowledgements This work was supported by the National Natural Science Foundation of China (Grant No. 12102374), the National Key Research and Development Program (Grant No. 2019YFE0120300), the Sichuan Science and Technology Program (Grant No. 2021YFH0031), the International Cooperation Project of Chengdu (Grant No. 2019-GH02-00054-HZ), and the Innovative Research Team of SWPU (Grant No. 2017CXTD01).

References

[1] Wang T, Zhang Y, Liu Q, et al. A self-healable, highly stretchable, and solution processable conductive polymer composite for ultrasensitive strain and pressure sensing. Advanced Functional Materials, 2018, 28(7): 1705551

[2] Wang L, Xiang D, Harkin-Jones E, et al. A flexible and multipurpose piezoresistive strain sensor based on carbonized phenol formaldehyde foam for human motion monitoring. Macromolecular Materials and Engineering, 2019, 304(12): 1900492

[3] He Y, Wu D, Zhou M, et al. Wearable strain sensors based on a porous polydimethylsiloxane hybrid with carbon nanotubes and graphene. ACS Applied Materials & Interfaces, 2021, 13(13): 15572–15583

[4] Zhang H, Liu D, Lee J H, et al. Anisotropic, wrinkled, and crack-bridging structure for ultrasensitive, highly selective multidirectional strain sensors. Nano-Micro Letters, 2021, 13(1): 122

[5] Wu X, Han Y, Zhang X, et al. Large-area compliant, low-cost, and versatile pressure-sensing platform based on microcrack-designed carbon black@polyurethane sponge for human-machine interfacing. Advanced Functional Materials, 2016, 26(34): 6246–6256

[6] Chen Q, Xiang D, Wang L, et al. Facile fabrication and performance of robust polymer/carbon nanotube coated spandex fibers for strain sensing. Composites Part A: Applied Science and Manufacturing, 2018, 112: 186–196

[7] Wang Y, Jia Y, Zhou Y, et al. Ultra-stretchable, sensitive and durable strain sensors based on polydopamine encapsulated carbon nanotubes/elastic bands. Journal of Materials Chemistry C: Materials for Optical and Electronic Devices, 2018, 6(30): 8160–8170

[8] Zhang M, Wang C, Wang Q, et al. Sheath–core graphite/silk fiber made by dry-meyer-rod-coating for wearable strain sensors. ACS Applied Materials & Interfaces, 2016, 8(32): 20894–20899

[9] Wang Y, Hao J, Huang Z, et al. Flexible electrically resistive-type strain sensors based on reduced graphene oxide-decorated electrospun polymer fibrous mats for human motion monitoring. Carbon, 2018, 126: 360–371

[10] Lan L, Jiang C, Yao Y, et al. A stretchable and conductive fiber for multifunctional sensing and energy harvesting. Nano Energy, 2021, 84: 105954

[11] Lee S, Shin S, Lee S, et al. Ag nanowire reinforced highly stretchable conductive fibers for wearable electronics. Advanced Functional Materials, 2015, 25(21): 3114–3121

[12] Xiang D, Zhang X, Harkin-Jones E, et al. Synergistic effects of hybrid conductive nanofillers on the performance of 3D printed highly elastic strain sensors. Composites Part A: Applied Science

and Manufacturing, 2020, 129: 105730

[13] Zheng Y, Li Y, Li Z, et al. The effect of filler dimensionality on the electromechanical performance of polydimethylsiloxane based conductive nanocomposites for flexible strain sensors. Composites Science and Technology, 2017, 139: 64–73

[14] Choi G, Jang H, Oh S, et al. A highly sensitive and stress-direction-recognizing asterisk-shaped carbon nanotube strain sensor. Journal of Materials Chemistry C: Materials for Optical and Electronic Devices, 2019, 7(31): 9504–9512

[15] Gao J, Li B, Huang X, et al. Electrically conductive and fluorine free superhydrophobic strain sensors based on SiO_2/graphene-decorated electrospun nanofibers for human motion monitoring. Chemical Engineering Journal, 2019, 373: 298–306

[16] Chen G, Wang H, Guo R, et al. Superelastic EGaIn composite fibers sustaining 500% tensile strain with superior electrical conductivity for wearable electronics. ACS Applied Materials & Interfaces, 2020, 12(5): 6112–6118

[17] Gao J, Wang L, Guo Z, et al. Flexible, superhydrophobic, and electrically conductive polymer nanofiber composite for multi-functional sensing applications. Chemical Engineering Journal, 2020, 381: 122778

[18] Yu S, Wang X, Xiang H, et al. Superior piezoresistive strain sensing behaviors of carbon nanotubes in one-dimensional polymer fiber structure. Carbon, 2018, 140: 1–9

[19] Yu S, Wang X, Xiang H, et al. 1-D polymer ternary composites: understanding materials interaction, percolation behaviors and mechanism toward ultra-high stretchable and super-sensitive strain sensors. Science China: Materials, 2019, 62(7): 995–1004

[20] Chen Y F, Li J, Tan Y J, et al. Achieving highly electrical conductivity and piezoresistive sensitivity in polydimethylsiloxane/multi-walled carbon nanotube composites via the incorporation of silicon dioxide micro-particles. Composites Science and Technology, 2019, 177: 41–48

[21] Yang Y, Zhao G, Cheng X, et al. Stretchable and healable conductive elastomer based on PEDOT:PSS/natural rubber for self-powered temperature and strain sensing. ACS Applied Materials & Interfaces, 2021, 13(12): 14599–14611

[22] Ma R, Lee J, Choi D, et al. Knitted fabrics made from highly conductive stretchable fibers. Nano Letters, 2014, 14(4): 1944–1951

[23] Qi K, Zhou Y, Ou K, et al. Weavable and stretchable piezoresistive carbon nanotubes-embedded nanofiber sensing yarns for highly sensitive and multimodal wearable textile sensor. Carbon, 2020, 170: 464–476

[24] Li Y, Zhou B, Zheng G, et al. Continuously prepared highly conductive and stretchable SWNT/MWNT synergistically composited electrospun thermoplastic polyurethane yarns for wearable sensing. Journal of Materials Chemistry C: Materials for Optical and Electronic Devices, 2018, 6(9): 2258–2269

[25] Gao Y, Guo F, Cao P, et al. Winding-locked carbon nanotubes/polymer nanofibers helical yarn for ultrastretchable conductor and strain sensor. ACS Nano, 2020, 14(3): 3442–3450

[26] Li B, Luo J, Huang X, et al. A highly stretchable, super-hydrophobic strain sensor based on polydopamine and graphene reinforced nanofiber composite for human motion monitoring. Composites Part B: Engineering, 2020, 181: 107580

[27] Xu Y, Xie X, Huang H, et al. Encapsulated core–sheath carbon nanotube–graphene/polyurethane composite fiber for highly stable, stretchable, and sensitive strain sensor. Journal of Materials Science, 2021, 56(3): 2296–2310

[28] Wang L, Chen Y, Lin L, et al. Highly stretchable, anti-corrosive and wearable strain sensors based on the PDMS/CNTs decorated elastomer nanofiber composite. Chemical Engineering Journal, 2019, 362: 89–98

[29] Yang Z, Zhai Z, Song Z, et al. Conductive and elastic 3D helical fibers for use in washable and wearable electronics. Advanced Materials, 2020, 32(10): 1907495

[30] Hu Y, Huang T, Zhang H, et al. Ultrasensitive and wearable carbon hybrid fiber devices as robust intelligent sensors. ACS Applied Materials & Interfaces, 2021, 13(20): 23905–23914

[31] Yue X, Jia Y, Wang X, et al. Highly stretchable and durable fiber-shaped strain sensor with porous core–sheath structure for human motion monitoring. Composites Science and Technology, 2020, 189(35): 108038

[32] Chen Q, Li Y, Xiang D, et al. Enhanced strain sensing performance of polymer/carbon nanotube-coated spandex fibers via noncovalent interactions. Macromolecular Materials and Engineering, 2020, 305(2): 1900525

[33] Cai J H, Chen Y F, Li J, et al. Asymmetric deformation in poly (ethylene-co-1-octene)/multi-walled carbon nanotube composites with glass micro-beads for highly piezoresistive sensitivity. Chemical Engineering Journal, 2019, 370: 176–184

[34] Cai J H, Li J, Chen X D, et al. Multifunctional polydimethylsiloxane foam with multi-walled carbon nanotube and thermo-expandable microsphere for temperature sensing, microwave shielding and piezoresistive sensor. Chemical Engineering Journal, 2020, 393: 124805

[35] Liu W, Yang Y, Nie M. Constructing a double-percolated conductive network in a carbon nanotube/polymer-based flexible semiconducting composite. Composites Science and Technology, 2018, 154: 45–52

[36] Bizhani H, Nayyeri V, Katbab A, et al. Double percolated MWCNTs loaded PC/SAN nanocomposites as an absorbing electromagnetic shield. European Polymer Journal, 2018, 100: 209–218

[37] Mao C, Zhu Y, Jiang W. Design of electrical conductive

composites: tuning the morphology to improve the electrical properties of graphene filled immiscible polymer blends. ACS Applied Materials & Interfaces, 2012, 4(10): 5281–5286

[38] Zhang X, Xiang D, Zhu W, et al. Flexible and high-performance piezoresistive strain sensors based on carbon nanoparticles@ polyurethane sponges. Composites Science and Technology, 2020, 200: 108437

[39] Singh N, Chand G, Kanagaraj S. Investigation of thermal conductivity and viscosity of carbon nanotubes–ethylene glycol nanofluids. Heat Transfer Engineering, 2012, 33(9): 821–827

[40] Socher R, Krause B, Müller M T, et al. The influence of matrix viscosity on MWCNT dispersion and electrical properties in different thermoplastic nanocomposites. Polymer, 2012, 53(2): 495–504

[41] Ji M, Deng H, Yan D, et al. Selective localization of multi-walled carbon nanotubes in thermoplastic elastomer blends: an effective method for tunable resistivity–strain sensing behavior. Composites Science and Technology, 2014, 92: 16–26

[42] Zhang S, Deng H, Zhang Q, et al. Formation of conductive networks with both segregated and double-percolated characteristic in conductive polymer composites with balanced properties. ACS Applied Materials & Interfaces, 2014, 6(9): 6835–6844

[43] Ma Z, Wei A, Li Y, et al. Lightweight, flexible and highly sensitive segregated microcellular nanocomposite piezoresistive sensors for human motion detection. Composites Science and Technology, 2021, 203: 108571

[44] Xiang D, Wang L, Tang Y, et al. Damage self-sensing behavior of carbon nanofiller reinforced polymer composites with different conductive network structures. Polymer, 2018, 158: 308–319

[45] Bao Y, Xu L, Pang H, et al. Preparation and properties of carbon black/polymer composites with segregated and double-percolated network structures. Journal of Materials Science, 2013, 48(14): 4892–4898

[46] Chen Y, Yang Q, Huang Y, et al. Influence of phase coarsening and filler agglomeration on electrical and rheological properties of MWNTs-filled PP/PMMA composites under annealing. Polymer, 2015, 79: 159–170

[47] Wang Y, Wang L, Yang T, et al. Wearable and highly sensitive graphene strain sensors for human motion monitoring. Advanced Functional Materials, 2014, 24(29): 4666–4670

[48] Xiang D, Zhang X, Li Y, et al. Enhanced performance of 3D printed highly elastic strain sensors of carbon nanotube/thermoplastic polyurethane nanocomposites via non-covalent interactions. Composites Part B: Engineering, 2019, 176: 107250